Adjoint-Based, CAD-Free Aerodynamic Shape Optimization of High-Speed Trains

Daria Jakubek and Claus Wagner

Abstract Following Othmer's work [14] on the continuous adjoint formulation for the computation of sensitivities of incompressible, steady-state, ducted flows, we will introduce an iterative, CAD-free, continuous, adjoint-based shape optimization procedure using gaussian filtered sensitivities and mesh morphing with radial basis function interpolation based on the approach described by [1, 2] for the optimization of the front part of the simplified model of a conceptual, generic high-speed train with respect to drag and pressure wave via single- and multi-objective optimization. We will show that, during pressure wave minimization, it was mainly the area with the widest sidewise extension in the bogie section which was affected by the strongest modifications while, on the other hand, for drag optimization the most sensitive areas and significant changes can be found in the front part of the nose tip section. First multi-objective investigations for two-dimensional testcases will show the influence of weighting and morphing parameters on the optimization process involving objective functions for drag and pressure wave.

1 Introduction

There are many different numerical strategies to improve the aerodynamic features of vehicles. Adjoint-based shape optimization techniques were significantly developed by Pironneau [17, 18] and Jameson [10, 11]. There are two different ways to use the adjoints in CFD: the discrete [5, 6, 12] and the continuous [15, 16] approach. According to [14] we will apply the continuous adjoints.

D. Jakubek (✉) · C. Wagner
German Aerospace Center (DLR), Institute of Aerodynamics and Flow Technology,
Simulation Center of Aerodynamic Research in Transportation (SCART),
Bunsenstraße 10, 37073 Göttingen, Germany
e-mail: daria.jakubek@dlr.de

C. Wagner
e-mail: claus.wagner@dlr.de

A. Dillmann et al. (eds.), *New Results in Numerical and Experimental Fluid Mechanics X*, Notes on Numerical Fluid Mechanics and Multidisciplinary Design 132, DOI 10.1007/978-3-319-27279-5_36

2 The Adjoint Approach

In our procedure, the solutions of primal and adjoint equations are iteratively used to calculate surface sensitivities, which are used to modify the shape of the investigated geometry during mesh morphing. The expression primal equations refers to the incompressible, steady RANS equations, which the adjoint equations are derived from. The adjoint equations and boundary conditions depend on the formulation of the optimization problem, i.e. the objective function. Let J be the objective function describing an aerodynamic property to be minimized. In most technical applications, these properties can be usually written as integrals of the pressure p and/or the flow velocity $\mathbf{u} = (u_1, u_2, u_3)$ in volumes Ω and/or on surfaces $\Gamma = \partial\Omega$.

$$J := \int\limits_{\Gamma} J_{\Gamma}\,(p, u_i)\,\mathrm{d}\Gamma + \int\limits_{\Omega} J_{\Omega}\,(p, u_i)\,\mathrm{d}\Omega \quad \longrightarrow \quad \min \tag{1}$$

State variables providing any minimum of J must, however, satisfy the state equations, which can be considered as additional constraints of the optimization problem. In this work, we want to focus on the optimization of incompressible, steady-state, turbulent flows around trains governed by the incompressible Reynolds-averaged Navier-Stokes (RANS) equations [14].

$$R_i := \frac{\partial}{\partial x_j}\left(u_i u_j + \delta_{ij}\, p - \nu_{\mathrm{eff}}\left(\frac{\partial u_i}{\partial x_j} + \frac{\partial u_j}{\partial x_i}\right)\right) = 0 \tag{2}$$

$$Q := -\frac{\partial\, u_j}{\partial x_j} = 0, \quad (i, j = 1, 2, 3) \tag{3}$$

The effective kinematic viscosity ν_{eff} is the sum of molecular and turbulent viscosity $(\nu + \nu_{\mathrm{t}})$. For incompressible flows with constant density ρ, p denotes the normalized, modified mean pressure $\left(\overline{p}/\rho + \frac{2}{3}k\right)$ and u_i the predicted Reynolds-averaged parts $(\overline{u}_i)$ of the instantaneous velocity $\overline{u}_i + u_i'$. The turbulent kinetic energy $k = \frac{1}{2}\overline{u_i' u_i'}$ is calculated from the fluctuating parts u_i'. The resulting constrained optimization problem can be solved by using the Lagrange function L [4]. The introduced Lagrange multipliers, or adjoint variables $\hat{\mathbf{u}} = \left(\hat{u}_1, \hat{u}_2, \hat{u}_3\right)$ and $\hat{p}$ are used to weight the constraints in Eqs. (2) and (3) to combine them with the cost function J:

$$L := J + \int\limits_{\Omega} \left[\left(\hat{u}_i\; R_i\right) + \left(\hat{p}\;\; Q\right)\right]\,\mathrm{d}\Omega \longrightarrow \min \tag{4}$$

The adjoint mean velocity $\hat{u}_i$ and the adjoint mean pressure $\hat{p}$ have to be chosen such that the variations of L wrt. the state variables $\mathbf{u} = (u_1, u_2, u_3)$ and p vanish.

$$\delta_{\mathbf{u}} L + \delta_p L = \delta_{\mathbf{u}} J + \delta_p J + \int\limits_{\Omega} \left[\hat{u}_i \left(\delta_{\mathbf{u}} R_i + \delta_p R_i\right) + \hat{p}\left(\delta_{\mathbf{u}} Q + \delta_p Q\right)\right] \mathrm{d}\Omega = 0 \quad (5)$$

Starting with the incompressible, steady RANS Eqs. (2) and (3) and taking into account the assumption of "frozen turbulence" ($\delta \nu_{\text{eff}} = 0$), integration by parts and the use of the divergence theorem leads to the incompressible, adjoint RANS equations

$$\hat{R}_i := \frac{\partial J_\Omega}{\partial u_i} - \left(\frac{\partial \hat{u}_i}{\partial x_j} + \frac{\partial \hat{u}_j}{\partial x_i}\right) u_j + \frac{\partial}{\partial x_j}\left(\delta_{ij}\hat{p} - \nu_{\text{eff}}\left(\frac{\partial \hat{u}_i}{\partial x_j} + \frac{\partial \hat{u}_j}{\partial x_i}\right)\right) = 0 \quad (6)$$

$$\hat{Q} := \frac{\partial J_\Omega}{\partial p} - \frac{\partial \hat{u}_i}{\partial x_i} = 0 \quad (7)$$

and the associated adjoint boundary conditions for walls and the inlet

$$\hat{u}_t = 0 \quad (8)$$

$$\hat{u}_n = -\frac{\partial J_\Gamma}{\partial p} \quad (9)$$

$$\frac{\partial \hat{p}}{\partial n} = 0 \quad (10)$$

and for the outlet

$$\hat{p} = \hat{\mathbf{u}} \cdot \mathbf{u} + \hat{u}_n u_n + \nu_{\text{eff}} (\mathbf{n} \cdot \nabla)\, \hat{u}_n + \frac{\partial J_\Gamma}{\partial u_n} \quad (11)$$

$$0 = u_n \hat{\mathbf{u}}_t + \nu_{\text{eff}} (\mathbf{n} \cdot \nabla)\, \hat{\mathbf{u}}_t + \frac{\partial J_\Gamma}{\partial \mathbf{u}_t} \quad (12)$$

where n and t label the surface normal/tangential components and $\partial/\partial n$ describes the surface normal gradient. The primal equations are used to calculate the primal state variables u_i and p. The solution of the adjoint equations provides the adjoint variables $\hat{u}_i$ and $\hat{p}$. The results are used to determine surface sensitivities via sensitivity analysis [14] which are used to evaluate the required shape modifications:

$$\frac{\partial L}{\partial n} = -\nu_{\text{eff}} \frac{\partial u_t}{\partial n} \frac{\partial \hat{u}_t}{\partial n} \quad (13)$$

The combination of filtered and smoothed surface sensitivities, preconditioned by a linear convolution filter with gaussian kernel [19], with surface-normal vectors provides the necessary surface modifications. During mesh morphing, radial basis function interpolation is used to transfer these surface modifications on the computational grid [1, 2, 7–9].

3 Objective Functions

In this paper we will discuss the optimization of two different features of train aerodynamics. We are using the objective functions for drag and pressure wave minimization and we combine them for multi-objective optimization.

3.1 Drag Optimization

The drag force $\mathbf{F} = (F_1, F_2, F_3)$ acting in the direction of $\mathbf{r} = (r_1, r_2, r_3)$ is calculated from the pressure and the viscous forces on the objective surface of the train Γ_{obj}:

$$J := F_i r_i = \int_{\Gamma_{\mathrm{obj}}} c_{\mathrm{dr}} \left(p\delta_{ij} - \tau_{ij} \right) n_j r_i \, \mathrm{d}\Gamma = \int_{\Gamma_{\mathrm{obj}}} J_\Gamma \, \mathrm{d}\Gamma, \tag{14}$$

where $\tau_{ij} = 2\nu_{\mathrm{eff}} \frac{1}{2} \left(\frac{\partial u_i}{\partial x_j} + \frac{\partial u_j}{\partial x_i} \right)$ describes the viscous stress tensor, $\nu_{\mathrm{eff}} = \nu + \nu_{\mathrm{t}}$ the effective viscosity and $\mathbf{n} = (n_1, n_2, n_3)$ the surface normal vector. For unit consistency reasons, we use an additional constant to modify the dimensions of the objective function so we can always use the same implementation of the adjoint multipliers $\hat{u}_i$ (m/s) and $\hat{p}_i$ $\left(\mathrm{m}^2/\mathrm{s}^2\right)$ in (4) with every objective function. In this case we use $c_{\mathrm{dr}} = 1$ (1/m s). This objective function is a surface integral and there are no contributions from the volume Ω. Consequently, the derivatives of J_Ω in (6) and (7) vanish. Nevertheless, the boundary conditions for $\hat{u}_i$ and $\hat{p}$ in (8)–(12) must be modified with the according derivatives of the objective function.

3.2 Pressure Pulse Optimization

At its nose and its tail a train generates a characteristical pressure wave with a positive and negative pressure peak [3]. For safety and security reasons, this pressure wave is one of the most important issues of train aerodynamics as it affects objects and structures around the train. In numerical investigations, the intensity of that pressure wave can be quantified by integrating the squared differences between the pressure p and the mean pressure p_{ref} over the volume cells Ω_{obj} along a straight line parallel to the track.

$$J := \int_{\Omega_{\mathrm{obj}}} \frac{c_{\mathrm{pw}}}{2} \left(p - p_{\mathrm{ref}}\right)^2 \mathrm{d}\Omega = \int_{\Omega_{\mathrm{obj}}} J_\Omega \mathrm{d}\Omega \tag{15}$$

Here, we use the constant $c_{\text{pw}} = 1\,\text{s/m}^2$. The pressure-wave objective function is a volume integral which is evaluated in the cells Ω_{obj} along the sampling line. Thus, we have to include the according derivatives of J_Ω needed in the adjoint Eqs. (6) and (7) while terms containing the derivatives of J_Γ vanish completely in (8)–(12) describing the adjoint boundary conditions.

3.3 Multi-Objective Optimization

There are different approaches for multi-objective optimization. The simplest way is to use the individual objective functions and just combine the sensitivities at each morphing step to evaluate one resulting shape modification for all objective functions involved. Another way is to run the optimization for a combined objective function. Here, we can either define a special function describing a physical effect related to and taking into account all the regarded aerodynamic features as a new, adapted objective function. This can be a hard search. A much easier way is to sum up the functions describing all the interesting flow characteristics. Especially if, like in our procedure, the objective functions always have the same dimensions for implementation reasons. On the other hand, the values of the different objective functions usually are not the same order. This can lead to unbalanced combinations, which in turn means that the optimization procedure will not lead to the desired combined optimum. To achieve a more balanced optimization, we can weight them with weighting factors b. In this paper, we combined the two described objective functions for pressure wave (15) and drag (14):

$$J := \int\limits_{\Gamma_{\text{obj}}} b_{\text{dr}} c_{\text{dr}} \left(p\delta_{ij} - \tau_{ij}\right) n_j r_i \,\mathrm{d}\Gamma + \int\limits_{\Omega_{\text{obj}}} \frac{b_{\text{pw}} c_{\text{pw}}}{2} \left(p - p_{\text{ref}}\right)^2 \,\mathrm{d}\Omega \tag{16}$$

4 Simulation Setup

The described continuous adjoint optimization procedure was applied on the conceptional Next Generation Train (NGT) developed at the German Aerospace Center DLR. For numerical simulations, we used a $1:25$ scaled model of the NGT. To reduce the computational effort, only the $l = 620\,\text{mm}$ long, $h = 176\,\text{mm}$ high and $w = 124\,\text{mm}$ wide front part was used for optimization, with the train floor 19.4 mm above ground. Details like wheels were omitted during the trial of the iterative optimization procedure. Figure 1 shows the CAD model of the NGT on the left and a part of the hybrid computational grid in the symmetry plane on the right. We used meshes with 2.7×10^6 cells for three-dimensional, and 21033 cells for two-dimensional simulations of incompressible, steady-state, viscous, turbulent flows, solving primal and adjoint RANS equations with the $k - \omega$ SST turbulence model

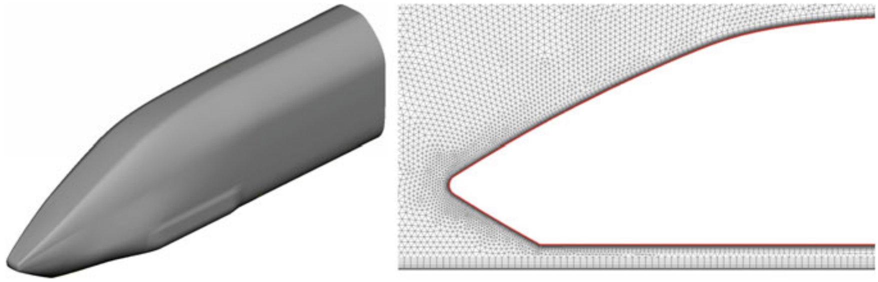

Fig. 1 CAD model of the NGT and the symmetry plane of the hybrid computational grid

for the primal equations and the frozen turbulence approximation for the adjoint equations. More detailed information about the grid and the simulation setup can be found in [8]. The specified Reynolds number $Re = 12.5 \times 10^4$ of the flow is based on the scaled reference length $l_{\mathrm{Re}} = 3/25$ m for trains and on the freestream velocity $u_x = 12.5$ m/s using the kinematic viscosity $\nu = 1.2 \times 10^{-5}$ m^2/s.

5 Optimized Train Shapes

For this study, we ran two-dimensional and three-dimensional testcases for single- and multi-objective drag and pressure wave optimization. By now, the multi-objective optimization procedure combining drag and pressure wave objective functions for high speed trains was only tested for two-dimensional testcases but it is currently being applied on three-dimensional configurations as well.

5.1 Two-Dimensional Testcases

For two-dimensional computations of the flow in the symmetry plane of the NGT we used a hybrid mesh consisting of 30358 grid points forming 21033 cells, 8100 of which belong to the structured boundary layer mesh.

5.1.1 Drag Optimization

Figure 2 shows the drag coefficient of four testcases with different morphing parameters, and the resulting optimal nose shapes. The drag coefficients were evaluated for the entire model, but shape optimization and mesh morphing have been applied to the nose tip section only, as this has turned out to be the most sensitive area in these testcases. The area shown in the small pictures on the right represents the deformation

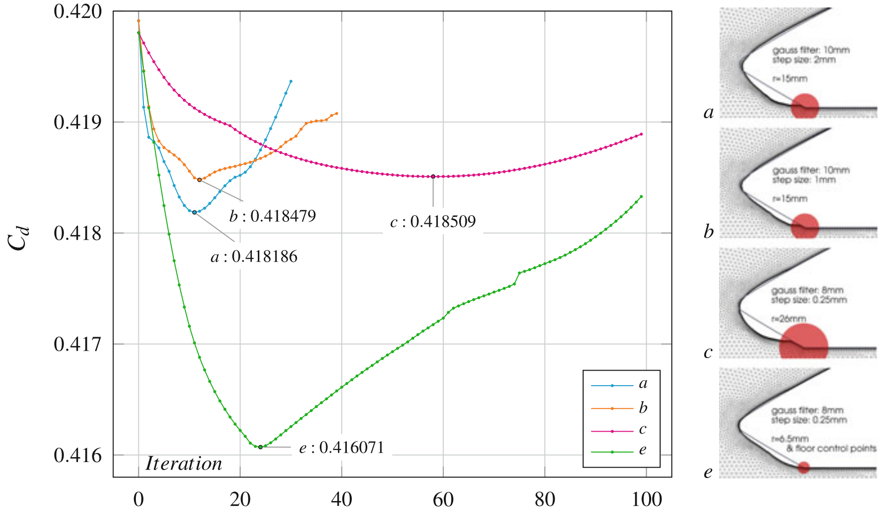

Fig. 2 Drag coefficient C_d for two-dimensional optimization with different sets of morphing parameters and control point distributions and the resulting optimum train nose shapes

area. For c and e, we used a smaller step size, leading to slower deformation, and the gaussian filter radius was 20 % smaller than for a and b. To preserve the train floor from being affected by the initiated mesh motion, for testcases a–c, we excluded the sensitivities in the area close the lower corner, with different radii defining the area of exclusion where mesh motion can drop to zero towards the edge. Another, more efficient strategy, was applied for testcase e, where additional zero-displacements were preset on the train floor to keep it fixed, independently from the other parameters. For all testcases, the drag coefficient drops constantly, but then starts to diverge after reaching a local minimum. Hence, the procedure requires a mechanism that controls the progress and stops the optimization when reaching a break condition. Further, the parameter studies reveal that choosing a smaller step size will damp and delay the divergence, as can be observed for c and e. In addition, sensitivities located close to edges must be handled with care. They should be smoothed properly and continuously distributed—if need be, by definition of additional zero-valued sensitivities for fixed surfaces e.g.

5.1.2 Pressure Wave Optimization

In three-dimensional train aerodynamics it is mainly the lateral effect of the pressure wave which is important. However, as there is no lateral dimension in two-dimensional simulations of a train, we decided to use the area above the NGT, 237 mm above ground, for the evaluation of the intensity of the generated pressure

Table 1 Two-dimensional pressure wave optimization: values of the objective function, Eq. (14)

Iteration	0	1	2	3	4	5	6
J_Γ ($\times 10^{-3}$)	6.19132	6.19052	6.19038	6.19027	6.19019	6.19014	6.19013

wave according to (15). Table 1 shows some values of the pressure wave objective function for two-dimensional optimization.

5.1.3 Multi-Objective Optimization

For multi-objective optimization, we combined the objective functions for drag and pressure wave according to Eq. (16). With $J_{\Gamma,0} = 5.772321 \times 10^{-3}$ and $J_{\Omega,0} = 6.19132 \times 10^{-3}$, i.e. $J_{\Gamma,0}/J_{\Omega,0} \approx 0.93$, the starting values of the contributing functions have the same order. To demonstrate the influence of weighting factors, we ran the optimization for $b_{\mathrm{dr}} = 1$ and different values of b_{pw}. Figure 3 shows the resulting nose shapes on the left and the values of the two objective functions on the right. As expected, with a small factor ($b_{\mathrm{pw}} = 0.0093$), the optimization yields a shape similar to a drag optimized geometry while, in contrast, an increased value of b_{pw} foregrounds the minimization of the pressure wave, which leads to different sensitivities and hence results in a different shape.

5.2 Three-Dimensional Testcases

For the three-dimensional optimization of the nose part of the NGT we used a hybrid mesh with 2.7 million cells. 350000 of these cells form the structured boundary layers around the train and at the ground.

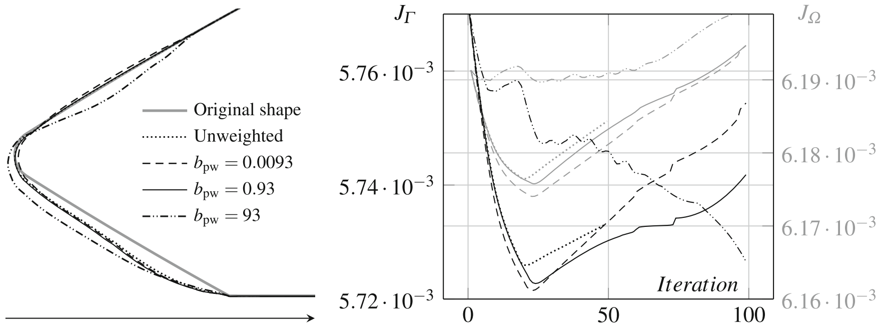

Fig. 3 Optimum shapes of the nose section for different balancing of $J = J_\Gamma + b_{\mathrm{pw}} \times J_\Omega$ and the development of the included objective functions during multi-objective optimization

Table 2 Three-dimensional drag optimization: values of the objective function, Eq. (14)

Iteration	0	1	2	3
J_{Γ} $(\times 10^{-2})$	7.43477	7.43425	7.43257	7.43239

5.2.1 Drag Optimization

During drag optimization for three-dimensional testcases we could obtain first results shown in Table 2. The procedure provides reduced drag coefficients but the step size of the deformations was chosen rather small to ensure good mesh quality so more iterations will be needed to achieve a higher reduction of the drag forces.

5.2.2 Pressure Wave Optimization

For three-dimensional pressure wave optimization of the NGT we used a line 0.12 m from the symmetry plane, 0.10 m above the ground, according to the procedures described in [3]. Figure 4 shows the extent of the accumulated modifications of the surface after five morphing steps. During mesh morphing, the maximum surface displacement for each morphing step was limited to the initial boundary layer thickness ($\delta_{BL_{init}} \sim 4.8$ mm). The largest resulting total deformations can be observed around the bulges in the lower part where they add up to 300 % of the initial boundary layer. As this objective function is defined and evaluated lateral of the train, and as it mainly depends on the displacement of the fluid flowing around the vehicle, it seems straightforward that the results of these calculations mostly aim for modifications in this part of the body with the largest lateral extension. Figure 5 reveals a consequent

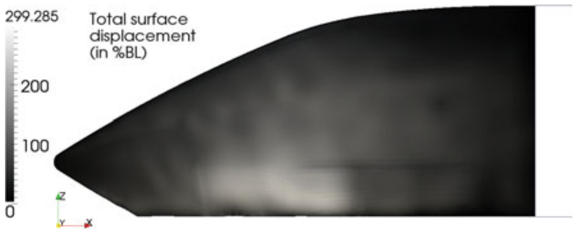

Fig. 4 Total surface displacements after five iteration steps of pressure wave optimization

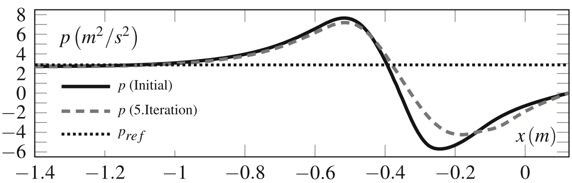

Fig. 5 Pressure pulse of the NGT and mean pressure p_{ref} (*dashed*) along the evaluation line generated after five cycles of the optimization process

Table 3 Three-dimensional pressure wave optimization: values of the objective function, Eq. (15)

Iteration	0	1	2	3	4	5
J_Ω	22.14	20.64	20.68	19.46	18.45	17.60

weakening of the pressure pulse in the evaluation area during the process and the results of the objective function shown in Table 3 confirm that observation. At the end of runtime the objective function could be reduced by a total of 20 %.

6 Summary

Based on the solutions of primal and adjoint Reynolds-Averaged Navier-Stokes (RANS) equations provided by the open source finite volume solver OpenFOAM [13], as suggested by Othmer [14], we introduced an iterative, CAD-free shape optimization process chain with the ability to be run automatically. Following the approach of de Boer [2] and Bos [1] we have developed a mesh morphing tool using gaussian filtering and radial basis function interpolation to calculate the new mesh. The process chain was designed to optimize the shape of an idealized model of the train head of the conceptional Next Generation Train (NGT), developed at the German Aerospace Center (DLR), with respect to single and multiple objective functions. We have applied the procedure to minimize the drag of the vehicle and the generated pressure wave in two- and three-dimensional testcases. The sensitivity analysis for pressure wave minimization have revealed that the most sensitive surface areas are located on the sides of the body close to the bogie sections. On the other hand, for drag optimization, it is rather the nose section which has the major influence on the objective function. For multi-objective optimization, we have combined these two objective functions by weighted summation. First results for two dimensional testcases have already provided optimized shapes while results for three-dimensional testcases will be available soon.

References

1. Bos, F.M.: Numerical simulations of flapping foil and wing aerodynamics—mesh deformation using radial basis functions. Ph. D. thesis, Technische Universiteit Delft (2009)
2. de Boer, A., van der Schoot, M.S., Bijl, H.: Mesh deformation based on radial basis function interpolation. Comput. Struct. **85**, 784–795 (2007)
3. CEN European Committee For Standardization: Railway applications—aerodynamics—part 4: requirements and test procedures for aerodynamics on open track. prEN 14067–4 (2011)
4. Feldmann, D.: Repetitorium der Ingenieur-Mathematik. Binomi Verlag, Hannover (1994)
5. Gauger, N.R.: Das Adjungiertenverfahren in der aerodynamischen Formoptimierung. Dissertation, Technische Universitöat Braunschweig, DLR Forschungsbericht 2003–2005 (2003)

6. Giles, M.B., Duta, M.C., Muller, J.-D., Pierce, N.A.: Algorithm developments for discrete adjoint methods. AIAA J. **41**(2), 198–204 (2003)
7. Jakubek, D., Wagner, C.: Shape optimization of train head cars using adjoint-based computational fluid dynamics. In: RAILWAYS 2012—The First International Conference on Railway Technology: Research, Development and Maintenance 2012. doi:10.4203/ccp.98.158
8. Jakubek, D., Herzog, S., Wagner, C.: Shape optimization of high speed trains using adjoint-based computational fluid dynamics. Int. J. railw. Technol. (2012). doi:10.4203/ijrt.1.2.4
9. Jakubek, D., Herzog, S., Wagner, C.: Adjoint-based shape optimization of high-speed trains. In: The Proceedings of the Engineering Optimization 2014. doi:10.1201/b17488-124
10. Jameson, A.: Aerodynamic design via control theory. J. Sci. Comput. **3**, 233–260 (1988)
11. Jameson, A.: Optimum Aerodynamic Design using CFD and Control Theory. AIAA-95–1729. In: The Proceedings of the 12th AIAA Computational Fluid Dynamics Conference, San Diego, California, USA, 19–22 Jun 1995
12. Nadarajah, S.K.: The discrete adjoint approach to aerodynamic shape optimization. Ph.D. Dissertation, Stanford University (2003)
13. Open FOAM: The open source CFD toolbox. Available via DIALOG. http://www.openfoam.com (2013). Accessed 20 Aug 2013
14. Othmer, C.: A continuous adjoint formulation for the computation of topological and surface sensitivities of ducted flows. Int. J. Numer. Meth. Fluids **58**, 861–877 (2008)
15. Othmer, C., de Villers, E., Weller, H.G.: Implementation of a continuous adjoint for topology optimization of ducted flows. AIAA-2007–3947. In: The Proceedings of the 18th AIAA Computational fluid dynamics conference, Miami, Florida, USA, 25–28 Jun 2007
16. Papadimitriou, D.I., Giannakoglou, K.C.: A continuous adjoint method with objective function derivatives based on boundary integrals for inviscid and viscous flows. Comput. Fluids **36**, 325–341 (2007)
17. Pironneau, O.: On optimum design in fluid mechanics. J. Fluid Mech. **64**, 97–110 (1974)
18. Pironneau, O.: Optimal Shape Design for Elliptic Systems. Springer, New York (1988)
19. Stueck, A.: Adjoint navier-stokes methods for hydrodynamic shape optimisation. Ph. D. thesis, TUHH, Hamburg (2011)